Quenching of OH(A 2 Σ +) by H 2 through Conical Intersections: Highly Excited Products in Nonreactive Channel

ARTICLE *in* THE JOURNAL OF PHYSICAL CHEMISTRY A · JUNE 2010

Impact Factor: 2.69 · DOI: 10.1021/jp1024069 · Source: PubMed

4 AUTHORS, INCLUDING:

Ruifeng Lu

Nanjing University of Science and Technol…

80 PUBLICATIONS **869** CITATIONS

SEE PROFILE

Quenching of OH($A^2\Sigma^+$) by H_2 through Conical Intersections: Highly Excited Products in Nonreactive Channel

Pei-Yu Zhang, Rui-Feng Lu, Tian-Shu Chu, and Ke-Li Han*

State Key Laboratory of Molecular Reaction Dynamics, Dalian Institute of Chemical Physics, Chinese Academy of Sciences, Dalian 116023, China

Received: March 16, 2010; Revised Manuscript Received: May 10, 2010

Nonadiabatic quantum scattering calculations have been carried out for the reactive and nonreactive quenching of OH($A^2\Sigma^+$) in collisions with molecular H_2 on two new potential energy surfaces of the 1A′ and 2A′ states. Integral cross sections of the reactive and nonreactive quenching channels and the quantum state distributions of the nonreactive channel have been obtained. The theory reveals a high degree of rotational excitation of the quenched OH($X^2\Pi$) products and vibrational excitation of the H_2 products. The calculated results are in good agreement with the existing experimental data. The topography of the potential energy surfaces in the conical intersection regions is provided in order to discuss the origin of the internal excitations of nonreactive products and the branching of the reactive and nonreactive channels.

I. Introduction

Hydroxyl radicals are important intermediates of many chemical processes in atmospheric and combustion chemistry. The OH + H_2 system is a prototype for understanding the collision dynamics of hydroxyl radicals and has become the most important four-atom benchmark.[1–3] There are seams of conical intersection between the ground state ($1^2A'$) and first excited state ($2^2A'$) for OH + H_2, and strong nonadiabatic coupling leads the OH($A^2\Sigma^+$) + H_2 to both H_2O + H (reactive quenching, RQ) and OH($X^2\Pi$) + H_2 (nonreactive quenching, NRQ) products.[4,5] As a result, it is also a sensible candidate for examining the nonadiabatic quenching processes through conical intersections.

In recent years, the study of this reaction has become one of the hot topics and many experimental studies have been reported.[1,5–15,28] Adiabatic potential energy surfaces (PESs) of the ground state $1^2A'$ have been theoretically constructed,[2,16,17,28] and numerous adiabatic dynamics calculations have been carried out on those PESs.[2,3,18–24,28] However, only few ab initio studies of exited states focused on the region of conical intersections.[4,5,8] As far as we know, no nonadiabatic quantum calculation has been published on the OH($A^2\Sigma^+$) + H_2 reaction. The increasing availability of experimental data underscores the need for quantum scattering dynamics calculations, which can accurately provide the detailed dynamics information. However, the theoretical calculations are extremely difficult because of the need for construction coupling PESs as well as nonadiabatic quantum scattering processes of the tetra-atomic systems.

Here we present a nonadiabatic quantum dynamics study on two PESs of the 1A′ and 2A′ states for the OH($A^2\Sigma^+$, $X^2\Pi$) + H_2 reaction. Because there is lack of realistic PESs with nonadiabatic coupling for this tetra-atomic system, PESs were first constructed with accurate ab initio data. Ab initio energies for all data points were calculated using the multireference configuration interaction (MRCI) scheme with the AVQZ basis set for the 1A′, 2A′, and 1A″ states. The technical details of construction of PESs are given in the Supporting Information (SI). The nonadiabatic time-dependent wave packet method is briefly described in Section II, whereas Section III presents the results of dynamical calculations and the comparison with experimental values. Section IV concludes.

II. Theory

The nonadiabatic quantum scattering approach for this system is the same as that in the previous work on the O_2+O_2 reaction.[25] The Hamiltonian for the diatom−diatom Hamiltonian reaction in the Jacobi coordinates can be written as

$$H = -\frac{\hbar^2}{2\mu}\frac{\partial^2}{\partial R^2} + \frac{(\hat{J} - \hat{J}_{12})^2}{2\mu R^2} + h_1(r_1) + h_2(r_2) + \frac{\hat{j}_1^2}{2\mu_1 r_1^2} + \frac{\hat{j}_2^2}{2\mu_2 r_2^2} + V(\vec{r}_1, \vec{r}_2, \vec{R}) \tag{1}$$

where

$$V = \begin{pmatrix} V_{11}^{\mathrm{d}} & V_{12}^{\mathrm{d}} \\ V_{21}^{\mathrm{d}} & V_{22}^{\mathrm{d}} \end{pmatrix} \tag{2}$$

is coupled diabatic potential energy matrix for two electronic states. The definitions of variables in Hamiltonian can be found in ref 29. The time-dependent wave function can be expressed as

$$\mathbf{\Psi}(\vec{r}_1, \vec{r}_2, \vec{R}; t) = \begin{pmatrix} \chi_1^{\mathrm{d}} \\ \chi_2^{\mathrm{d}} \end{pmatrix} \tag{3}$$

χ_1^{d} and χ_2^{d} correspond to wave functions on each of the two diabatic PESs, respectively, and $\chi_i^{\mathrm{d}}(i = 1, 2)$ are expanded in terms of translational basis, vibrational basis, and body-fixed total angular momentum eigenfunction.[29] The wave function is propagated by extended split-operator scheme[30,31]

* Corresponding author. E-mail: klhan@dicp.ac.cn. Tel: +86-0411-84379293. Fax: +86-411-84675584.

10.1021/jp1024069
Published on Web 05/26/2010

$$\Psi(\vec{r}_1, \vec{r}_2, \vec{R}; t + \Delta) =$$

$$e^{-iH_0 I\Delta/2} e^{-iV_{rot} I\Delta/2} \exp\left(-i\begin{pmatrix} V_{11}^d & V_{12}^d \\ V_{21}^d & V_{22}^d \end{pmatrix}\Delta\right) \Delta e^{-iV_{rot} I\Delta/2} e^{-iH_0 I\Delta/2} \Psi(\vec{r}_1, \vec{r}_2, \vec{R}; t) \quad (4)$$

H_0 and V_{rot} are the reference Hamiltonian and rotational part of Hamiltonian, respectively.[29] I is a 2 × 2 identity matrix, and

$$\exp\left(-i\begin{pmatrix} V_{11}^d & V_{12}^d \\ V_{21}^d & V_{22}^d \end{pmatrix}\Delta\right) = \mathbf{T}\begin{pmatrix} \exp(-iV_1^{ad}\Delta) & 0 \\ 0 & \exp(-iV_2^{ad}\Delta) \end{pmatrix}\tilde{\mathbf{T}}^+ \quad (5)$$

where $V_i^{ad}(i = 1, 2)$ are the adiabatic electronic energies and **T** is the eigenvector matrix of diagonalization. Finally, the initial state specified total reaction probabilities are obtained by flux operator for each of the electronic states, and the reaction cross section is calculated by summing the reaction probabilities over all partial waves (total angular momentum, J).[29]

The parameters used in the calculation are as follows. We employed 458 sine functions (among them, 90 for the interaction region) for the diatom−diatom distance in a range of [2, 16] bohrs, and 45 vibrational functions of H_2 were employed for r_{HH} in the range of [0.6, 6.0] bohrs for the interaction region. The maximum rotational state j_{max} =16 and 28 for the H_2 and OH, respectively. Seven and five vibrational states are included in the asymptotic region for the H_2 and OH, respectively. The initial translational energy, width, and center of initial wave packet are 0.35 eV and 0.3 and 8 bohrs. The time step was 15 au and the total propagation time was 30 000 au. Calculated integral cross section are well converged with the used basis functions. The initial-state-selected calculations are performed at rovibrational ground states of reactants OH($A^2\Sigma^+$) and H_2 for total angular momentum J values up to 70.

III. Results and Discussion

Complete vibrational and rotational distributions of OH(X^2II) products in the NRQ channel are presented in Figure 1. It is clear that the OH(X^2II) products are highly rotationally excited at all collision energies. With decreasing collision energy from 0.30 to 0.06 eV, the rotational distribution of OH(X^2II) becomes slightly narrower with a peak of the rotational distribution at j' = 15−17, and the average rotational energy decreases from 4624 to 3790 cm^{-1}. Figure 1 also shows the experimental results of Lester and coworkers.[6,9] They investigated the rotational distribution and found a narrow rotational distribution with a peak at j' = 15 for OH(X^2II) ground vibrational state with an average rotational energy of 3720 ± 100 cm^{-1}. The theoretical rotational distribution has the same peak at 15 in v'_1 = 0 for the collision energy E = 0.06 eV with the average rotational energy of 3790 cm^{-1}. The theoretical distributions agree well with the experimental results because the experimental results are obtained at an low temperature of ∼50 K.[6,9] To explore the origin of this highly rotational excitation, views of fitted PESs with T-shaped and linear geometries of the conical intersection are shown in Figure 2a and Figure S2a of the Supporting

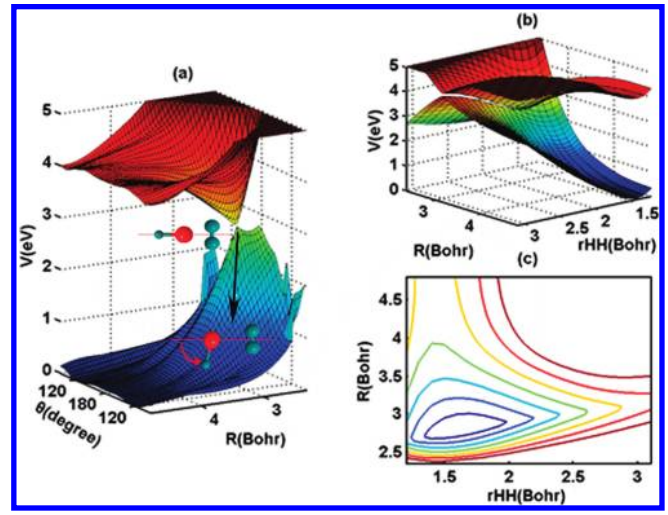

Figure 2. Plots of fitted potential surfaces for T-shaped configurations. The geometry of OH + H_2 system is defined by the coordinates R, r_1, r_2, θ_{OH}, and θ_{HH} in Figure S1 of the Supporting Information. θ_{HH} = 90° for T-shaped configurations. (a) 3D perspective as a function of R and the angle θ_{OH}. The bond lengths of OH, r_{OH} = 1.833 bohrs, and bond lengths of H_2 r_{HH} =1.4 bohrs were fixed. (b) 3D perspective as a function of R and r_{HH}, and r_{OH} = 1.833 bohrs, θ_{OH} =180°. (c) Contour map of upper surface in part b.

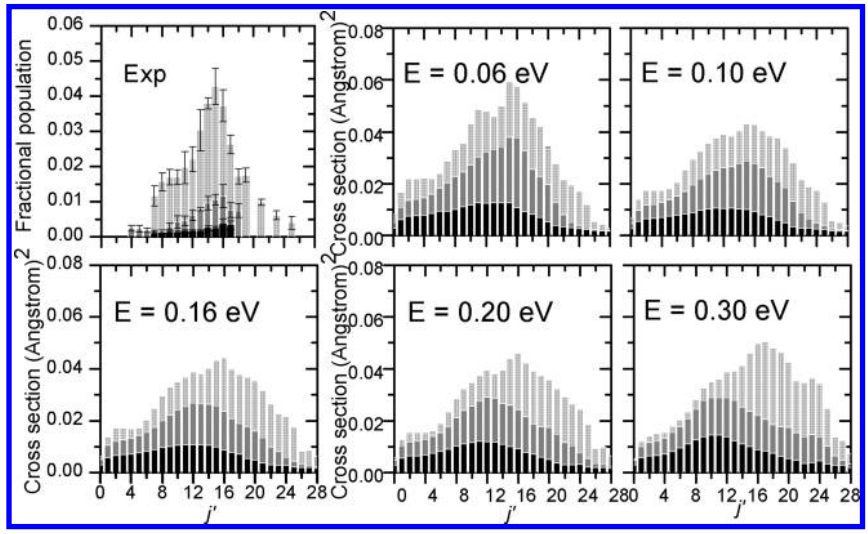

Figure 1. Vibrational and rotational state distributions for OH($A^2\Sigma^+$) + H_2 → OH(X^2II) (v'_1 = 0−2, j'_1) + H_2 as a function of j'_1 at different collision energies. The histograms for the vibrational levels (v'_1 = 0−2) of the OH(X^2II) are light gray, gray, and black, respectively. The first panel shows the experimental results with the uncertainty estimates.[6,9]

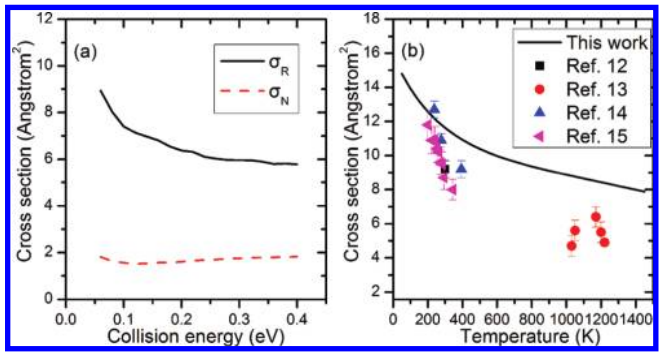

Figure 3. (a) Calculated integral cross sections for reactive quenching (σ_R) and nonreactive quenching (σ_N) as a function of collision energy. (b) Temperature-dependent cross section $\sigma(T)$ together with the previous experimental results.

Information. The geometry is defined by the coordinates R, r_1, r_2, θ_{OH}, and θ_{HH} in Figure S1 of the Supporting Information. For the same distance R, the energy of $1^2A'$ is a maximum at $\theta_{OH} = 180°$ and decreases significantly with decreasing θ_{OH}. On the contrary, the energy of $2^2A'$ is smallest at $\theta_{OH} = 180°$ and increases significantly with decreasing θ_{OH}. Therefore, this steep angular gradient of θ_{OH} away from the conical intersection, which is consistent with the ab initio results of Cleary et al. and Hoffman et al.,[4,8] is expected to lead to rotational excitation of the electronically quenched OH products.

On the other hand, the theory shows little vibrational excitation of OH($X^2\Pi$) product and highly vibrational excitation of H_2 product. (See Table S1 of the Supporting Information.) The vibrational excitations of the OH($X^2\Pi$) product are relatively invariant to collision energy. At a collision energy of 0.06 eV, the theoretical vibrational state distributions are 0.539, 0.329, and 0.133 for $v'_1 = 0$ to 2, respectively. The corresponding experimental values are 0.726, 0.218, and 0.056.[7] The product H_2 is highly vibrationally excited up to $v'_2 = 6$. This vibrational excitation of H_2 comes about because of the dependence of the $2^2A'$ PES on the H_2 distance r_{HH} in the regions of conical intersection. Shown in Figures 2b and S2b is a 3D perspective of the $1^2A'$ and $2^2A'$ PESs associated with the T-shaped structures and linear structures, respectively. As seen in Figures 2b,c and S2b,c, the minimal energies of the conical intersections of $2^2A'$ are -1.94 eV for the linear geometry and -1.36 eV for the T-shaped geometry relative to the energy of dissociation limit OH($A^2\Sigma^+$) + H_2. The r_{HH} of bottom of the potential well of $2^2A'$ is 1.78 bohrs for the linear geometry and 1.62 bohrs for the T-shaped geometry, respectively. When the reactants of the OH($A^2\Sigma^+$,$X^2\Pi$) + H_2 system pass through these regions, H_2 will be stretched from the equilibrium distance ($r_{HH} = 1.4$ bohrs).

Figure 3a shows the reaction cross section as a function of the collision energy. The cross section of reactive quenching (σ_R) decreases with the collision energy, whereas the cross section of NRQ (σ_N) varies little with the increasing collision energy. It is found that the dominant process is reactive quenching forming H_2O + H. The theory predicted a 0.168 to 0.239 branching fraction of NRQ products at collision energies of 0.06 and 0.4 eV, with an increase trend over the whole energy range, which is consistent with the experimental prediction of 0.12 ± 0.05 at the low temperature of ~50 K.[7] The time evolution of probability density near the conical intersections is analyzed to find out the reason of preference in reactive quenching channel for the reaction. Figure 4 reveals that at most of the propagation time, the biggest probability densities occur nearby the linear configurations ($\theta_{OH} = 180°$ and $\theta_{HH} = 0°$), and the probability density decreases rapidly with the increasing θ_{HH} and decreasing θ_{OH}. At the propagation time of 2400 au, there is the most probability density, with the density of linear configuration about 169 times bigger than that of T-shaped configuration. Coming back to Figures 2b and S2b, it can be seen that compared with the T-shaped conical intersection with $R = 2.78$ bohrs, the geometry of the linear conical intersection ($R = 3.18$ bohrs) is much closer to that of the reactants, with deeper potential energy well. Also seen from Figures 2b and S2b, moving the OH-H_2 collision pair from the conical intersection to the two regions with small and large, respectively, R will lead to products of the RQ and NRQ channels, respectively. The gradient from the T-shaped conical intersection to smaller R is smaller than that in the opposite direction. As a result, if we put the OH-H_2 collision pair on the point of the T-shaped conical intersection and consider the reaction in the limit of no translational energy of the OH-H_2 collision pair, the favorable products would be OH + H_2 rather than H_2O + H. In contrast, the difference of gradients for RQ and NRQ channels in the linear conical intersection region is not so obvious. This topography of T-shaped and linear conical intersection is consistent with the investigation of gradient directed paths leading away from the conical intersection by Hoffman et al.[4]

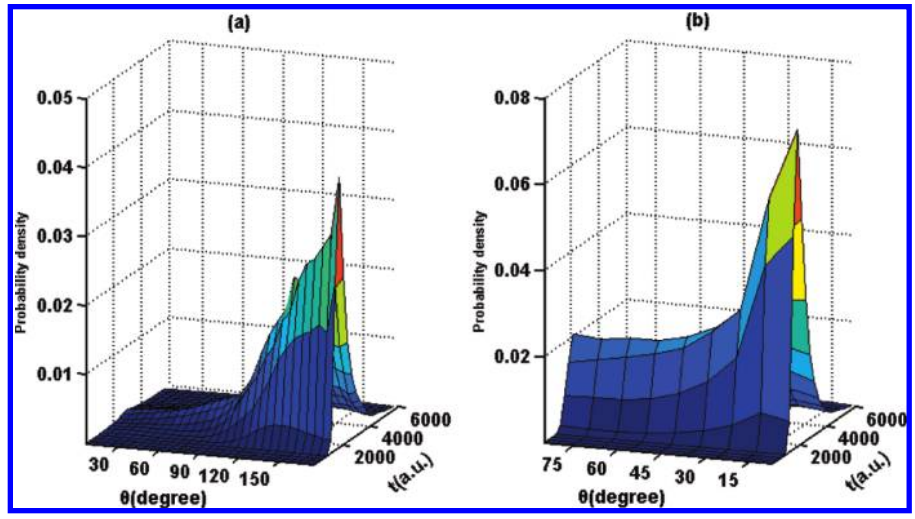

Figure 4. Time-dependent probability density integrated nearby the conical intersections as a function of θ_{OH}, and θ_{HH}, respectively. The calculation are performed for the total angular momentum $J = 0$.

Therefore, such preference of the wavepacket propagation through the linear conical intersection shown in Figure 4 decreases the products of NRQ channel.

Depicted in Figure 3b is the corresponding initial-state-selected temperature-dependent cross section $\sigma(T)$ together with the previous experimental results. The theoretical and experimental cross sections both decrease with increasing temperature. The decreasing trend of temperature-dependent cross sections indicates attractive forces dominating the collision process. The computed $\sigma(T)$ deviates from the experimental values with increasing temperature. Note that the theoretical $\sigma(T)$ involves only the results of rovibrational ground states of reactants $OH(A^2\Sigma^+)$ and H_2 without averaging over initial rotations of the reagents. However, as temperature increases, the experimental rotational distribution $OH(A^2\Sigma^+)$ shifts to higher rotational state j, and the most probable value of j at 1200 K is 4.5.[26] The rotational-level dependence of $OH(A^2\Sigma^+)$ quenching has been studied by Copeland et al.[27] The experimental data $\sigma_{exp}(T)$ at 294 K are 11.6, 9.0, 8.2, 7.3, and 6.5 Å for rotational numbers of reactant $OH(A^2\Sigma^+)$ $j = 0$, 1, 3, 4, 5, and 6, respectively. Therefore, $\sigma_{exp}(j = 0)/\sigma_{exp}(j = 4) = 1.41$ and $\sigma_{exp}(j = 0)/\sigma_{exp}(j = 5) = 1.59$. Assuming that the ratios of cross sections among different j do not vary with temperature, the computed initial-state-selected cross sections for $j = 0$ should be bigger than the experimental result $\sigma_{exp}(j \approx 4.5)$ by the factors of 1.41 to 1.59 at 1200 K. As shown in Figure 3b, the computed value at $j = 0$ is $\sigma(j = 0) = 8.46$ Å, and $\sigma(j = 0)/\sigma_{exp}(j \approx 4.5) = 1.57$. Therefore, considering the initial rotational distribution of reactant $OH(A^2\Sigma^+)$ in experiment, the theoretical temperature-dependent cross sections are in good agreement with the experimental measurement. However, a number of nonadiabatic dynamics with different initial rotations of the reagent $OH(A^2\Sigma^+)$ should be performed in the future to verify whether the above assumption is appropriate.

IV. Summary

In this work, we have presented a nonadiabatic quantum scattering study of reactive and nonreactive quenching of $OH(A^2\Sigma^+)$ in collisions with molecular H_2. As far as we know, this is the first work carrying out the nonadiabatic scattering calculation of the quenching process via the conical intersection of the tetra-atomic system. The theory reveals a high degree of rotational excitation of quenched $OH(X^2\Pi)$ products and vibrational excitation of the H_2 products in the nonreactive channel. These quantum-state distributions are found to be dominated by the topography of the PESs in the conical intersection regions. Therefore, the calculation provides fruitful information for understanding quenching processes through conical intersections in chemical reaction.

Acknowledgment. We thank Prof. Marsha Lester for discussions and for sending experimental data. This work was supported by NKBRSF (2007CB815202) and NSFC (20833008).

Supporting Information Available: Details of the methods used in this work and additional results. This material is available free of charge via the Internet at http://pubs.acs.org.

References and Notes

(1) Strazisar, B. R.; Lin, C.; Davis, H. F. *Science* **2000**, *290*, 958–961.
(2) Schatz, G. C.; Elgersma, H. A. *Chem. Phys. Lett.* **1980**, *73*, 21–25.
(3) Clary, D. C. *J. Phys. Chem.* **1994**, *98*, 10678–10688.
(4) Hoffman, B. C.; Yarkony, D. R. *J. Chem. Phys.* **2000**, *113*, 10091–10099.
(5) Lester, M. I.; Loomis, R. A.; Schwartz, R. L.; Walch, S. P. *J. Phys. Chem. A* **1997**, *101*, 9195–9206.
(6) Dempsey, L. P.; Murray, C.; Cleary, P. A.; Lester, M. I. *Phys. Chem. Chem. Phys.* **2008**, *10*, 1424–1432.
(7) Dempsey, L. P.; Murray, C.; Lester, M. I. *J. Chem. Phys.* **2007**, *127*, 151101.
(8) Cleary, P. A.; Dempsey, L. P.; Murray, C.; Lester, M. I.; Klos, J. *J. Chem. Phys.* **2007**, *126*, 204316–204327.
(9) Dempsey, L. P.; Sechler, T. D.; Murray, C.; Lester, M. I.; Matsika, S. *J. Chem. Phys.* **2009**, *130*, 104307.
(10) Ortiz-Suarez, M.; Witinski, M. F.; Davis, H. F. *J. Chem. Phys.* **2006**, *124*, 201106.
(11) Hemming, B. L.; Crosley, D. R. *J. Phys. Chem. A* **2002**, *106*, 8992–8995.
(12) Kenner, R. D.; Capetanakis, F. P.; Stuhl, F. *J. Phys. Chem.* **1990**, *94*, 2441–2446.
(13) Heard, D. E.; Henderson, D. A. *Phys. Chem. Chem. Phys.* **2000**, *2*, 67–72.
(14) Copeland, R. A.; Crosley, D. R. *J. Chem. Phys.* **1986**, *84*, 3099–3105.
(15) Smith, G. P.; Crosley, D. R. *J. Chem. Phys.* **1986**, *85*, 3896–3901.
(16) Wu, G.; Schatz, G. C.; Lendvay, G.; Fang, D. C.; Harding, L. B. *J. Chem. Phys.* **2000**, *113*, 3150–3161.
(17) de Aspuru, G. O.; Clary, D. C. *J. Phys. Chem. A* **1998**, *102*, 9631–9637.
(18) Manthe, U.; Matzkies, F. *J. Chem. Phys.* **2000**, *113*, 5725–5731.
(19) Zhang, D. H.; Zhang, J. Z. H. *J. Chem. Phys.* **1994**, *100*, 2697–2706.
(20) Bradley, K. S.; Schatz, G. C. *J. Phys. Chem.* **1994**, *98*, 3788–3795.
(21) Wang, D. S.; Bowman, J. M. *J. Chem. Phys.* **1992**, *96*, 8906–8913.
(22) Schatz, G. C. *J. Chem. Phys.* **1981**, *74*, 1133–1139.
(23) Schatz, G. C. *J. Phys. Chem.* **1995**, *99*, 516–524.
(24) Wang, D. S. *J. Chem. Phys.* **1993**, *98*, 6235–6247.
(25) Zhang, P. Y.; Lu, R. F.; Zhang, A. J.; Chu, T. S.; Han, K. L. *J. Chem. Phys.* **2008**, *128*, 091103.
(26) Crosley, D. R. *J. Phys. Chem.* **1989**, *93*, 6273–6282.
(27) Copeland, R. A. *J. Chem. Phys.* **1985**, *82*, 4022–4032.
(28) Kamarchik, E.; Fu, B.; Bowman, J. M. *J. Chem. Phys.* **2010**, *132*, 091102.
(29) Zhang, J. Z. H. *Theory and Application of Quantum Molecular Dynamics*; World Scientific: Singapore, 1999.
(30) Chu, T. S.; Zhang, Y.; Han, K. L. *Int. Rev. Phys. Chem.* **2006**, *25*, 201.
(31) Xie, T. X.; Zhang, Y.; Zhao, M. Y.; Han, K. L. *Phys. Chem. Chem. Phys.* **2003**, *5*, 2034.

JP1024069